Available online at www.sciencedirect.com
ScienceDirect
Journal of Power Sources 181 (2008) 207–213
JOURNAL OF POWER SOURCES
www.elsevier.com/locate/jpowsour

Investigation of the protonic conduction in Sm doped $BaCeO_3$

E. Gorbova [a], V. Maragou [b], D. Medvedev [a], A. Demin [a,1], P. Tsiakaras [b,*]

[a] *Institute of High Temperature Electrochemistry, 22 S.Kovalevskoy, 620219 Yekaterinburg, Russia*
[b] *School of Engineering, Department of Mechanical Engineering, University of Thessaly, Pedion Areos, 383 34 Volos, Greece*

Received 30 September 2007; received in revised form 18 January 2008; accepted 21 January 2008
Available online 1 February 2008

Abstract

In the present work the structural and electrical properties of samarium-doped barium cerate perovskites of $BaCe_{1-x}Sm_xO_{3-\delta}$ formula (with $x = 0$–0.2), prepared by following the solid state reaction method, are investigated. The crystal structure and microstructure of the samples is determined by employing the techniques of X-ray Diffraction (XRD) and Scanning Electron Microscopy (SEM). According to the XRD analysis at $0 \le x \le 0.2$ the formed continuous series of $BaCe_{1-x}Sm_xO_{3-\delta}$ solid solutions have the structure of cubic perovskite with orthorhombic distortions. It was found that the relative density of the samples is ~87% for $0.02 < x < 0.05$ and ~94% for $0.05 < x < 0.25$. It was also found that the highest conductivity is observed for $x = 0.15$. Finally, the thermal expansion of $BaCe_{1-x}Sm_xO_{3-\delta}$ ($x = 0$–0.2) is studied and the thermal expansion coefficients for the high temperature region are calculated.
Published by Elsevier B.V.

Keywords: Samarium doped barium cerates; Protonic conductors; Electrical conductivity; Perovskite

1. Introduction

Doped barium cerate ($BaCeO_3$) materials are considered as promising electrolytes for solid oxide fuel cells (SOFCs) operating at low and intermediate temperatures. The protonic conductivity of these materials and their application in SOFCs were first investigated by Iwahara et al. [1,2], although the cubic $BaCeO_3$ structure and its orthorhombic phase [3,4] were reported decades earlier. The structural phase transitions of $BaCeO_3$ have been investigated by Knight [5] who found a three structural phase transitions of $BaCeO_3$; with the increase of temperature the crystal structure changes from orthorhombic *Pmcn* to orthorhombic *Incn* at 563 K, the first-order transition from *Incn* to rhombohedral *F*32/*n* at 673 K and the second-order one from rhombohedral to cubic *Pm*3*m* at 1173 K. Recently, many studies have been devoted to the investigation of the doped barium cerates' structure, transport properties and chemical stability [6–12], as well as to their application in fuel cells [13–20].

Barium cerates $BaCe_{1-x}R_xO_{3-\delta}$, doped in the cerium position by R^{3+} (where R^{3+} represents a cation of rare-earth element) belong to a group of electrolytes that exhibit protonic conduction [21]. It is known that temperature and atmosphere influence the transport properties of most of the ionic conductors.

The incorporation of trivalent dopants into the $BaCeO_3$ structure, results in the introduction of oxygen vacancies, which react in turn with oxygen to produce electron holes in an oxygen rich atmosphere, as follows:

$$2Ce_{Ce}^{X} + O_o^X + M_2O_3 \rightarrow 2M'_{Ce} + V_o^{\bullet\bullet} + 2CeO_2 \quad (1)$$

$$\frac{1}{2}O_2 + V_o^{\bullet\bullet} \overset{K_1}{\longleftrightarrow} O_o^x + 2h^{\bullet} \quad (2)$$

At the first stage, a number of authors suggested the following mechanism of proton conductivity appearance in a hydrogen/water rich atmosphere [22,23]:

$$H_2O + V_o^{\bullet\bullet} \leftrightarrow 2H_i^{\bullet} + O_o^x \quad (3)$$

Afterwards, the following mechanism was proposed for the incorporation of protons [24,25]:

$$H_2O + V_o^{\bullet\bullet} + O_o^X \overset{K_2}{\longleftrightarrow} 2OH_o^{\bullet} \quad (4)$$

* Corresponding author. Tel.: +30 24210 74065; fax: +30 24210 74050.
E-mail addresses: A.Demin@ihte.uran.ru (A. Demin), tsiak@uth.gr (P. Tsiakaras).
[1] Tel.: +7 3432 745431; fax: +7 3432 745992.

0378-7753/$ – see front matter. Published by Elsevier B.V.
doi:10.1016/j.jpowsour.2008.01.036

Proton is a positively charged elementary particle, whose size is vanishingly small compared with other lattice ions. In the lattice of oxides, the proton is localized near an oxygen ion [26–28]; moreover, it inserts itself in the electron sheath of the oxygen ion [29]. Thus, an interstitial proton may be represented as an OH^- group that occupies an oxygen point, i.e. $OH_o^\bullet$ [30]. In the work of Scherban et al. [31] the presence of OH group in the $BaCeO_3$ lattice was found by infrared spectroscopy.

In general, the conductivity in mixed conductors is related to defects acting as effective charge carriers [32], which in this case consist of oxygen vacancies, electron holes and protons, leading to oxygen ion, electronic and proton conductivity, respectively:

$$\sigma_{\text{Total}} = \sum \sigma_i = \sum q_i C_i B_i \quad (5)$$

where σ_i is the conductivity component contributed by charge carrier species i, C_i is the concentration of the charge carrier, q_i is the charge and B_i is the mobility of charge carrier species i. The latter is mainly affected by temperature only, while by modifying the composition or the suitable physical parameters capable of varying the defect concentrations, the transport properties can be enhanced.

The concentration of protons can be derived from Eq. (3) according to [33]:

$$[H^\bullet] = K^{1/2}[V_o^{\bullet\bullet}]^{1/2} P_{H_2O}^{1/2} \quad (6)$$

where K is the equilibrium constant of Eq. (3), $[H^\bullet]$ and $[V_o^{\bullet\bullet}]$ are the concentrations of protons and oxygen vacancies, and P_{H_2O} the partial pressure of water vapor.

As mentioned above, doped barium cerates ($BaCe_{1-x}R_xO_{3-\delta}$) can be used as electrolytic materials in solid oxide fuel cells [34]. One of the advantages of these materials' use in SOFCs is the higher obtained efficiency in comparison with the efficiency of the oxygen-ion electrolyte based ones [35–37]. Moreover, proton conduction in $BaCeO_3$ follows the hopping mechanism, which results in lower activation energy due to the small size of proton [38]. Additionally, the electronic conductivity of barium cerates is much lower than that of other solid electrolytes, for example, doped ceria under the operating conditions, and thus, the cell EMF, power output and conversion efficiency could be significantly improved [39].

A number of works with respect to $BaCeO_3$ based oxides have already been published [40–42]; however, with remarkable differences in the reported conduction properties among them. Although the factors affecting the conduction properties of this type of electrolyte are very complex, it may be considered that its properties are influenced by the type and the content of the dopant, as well as by the preparation method of this material. Usually, in order to prepare a doped barium cerate powder, the conventional solid state reaction method is used, consisting of calcining mixtures of the initial materials in the form of oxides and carbonates at elevated temperatures (≥1000 °C), followed by sintering the powder compacts at 1600 °C [43].

One of the possible dopants for barium cerates is samarium. In the literature, there are only few works devoted to the preparation [44–46] and utilization of this material in SOFCs [46–49]. Initially, the majority of tests were made using single fuel cells based on barium cerate with Pt or Ag electrodes and sometimes with Ni anodes [34]. Recently, many researchers have investigated the operation of single fuel cells with electrodes of base metals [46,47,50]. Iwahara et al. [46] studied hydrogen-air fuel cells based on samarium-doped barium cerate using various oxides as the cathode and porous nickel as the anode. In the work of Ranran et al. [47] it was demonstrated that the maximum power density of 340 mW cm^{-2} was obtained at 700 °C, using the single cell with the $BaCe_{0.8}Sm_{0.2}O_{2.9}$ (BCSO) electrolyte of 50 μm in thickness, with $Ba_{0.5}Sr_{0.5}Co_{0.8}Fe_{0.2}$-BSCO as the cathode and Ni-BCSO as the anode. The conductivity of $BaCe_{0.8}Sm_{0.2}O_{2.9}$ under the cell operating conditions was 0.00938 S cm^{-1} at 700 °C. Kuzin et al. [50] have also studied the electrochemical characteristics of a single fuel cell based on $BaCe_{0.9}Nd_{0.1}O_{3-\delta}$ electrolyte with non-precious electrodes (nickel-cermet anode and $La_{0.8}Sr_{0.2}MnO_3$ cathode). In the work of Maffei et al. [14] the operation of a direct ammonia fuel cell utilizing a $BaCe_{0.8}Gd_{0.15}Pr_{0.05}O_3$ solid electrolyte was investigated employing $BaCe_{0.85}Eu_{0.15}O_3$ and Ni cermet as the anode.

Hibino et al. [51] investigated the performance of a 3wt% Pd-loaded FeO/25 mol% Y^{3+}-doped $BaCeO_3$/$Ba_{0.5}Pr_{0.5}CoO_3$ solid oxide fuel cell in the temperature range of 350–600 °C. It was found that the overpotentials of the Pd-loaded FeO anode and the $Ba_{0.5}Pr_{0.5}CoO_3$ cathode at 600 °C were less than one-fourth those of a Pt electrode. Moreover, the BCY25 electrolyte exhibited higher ion conductivities than 8 mol% yttria-stabilized zirconia below 800 °C and 20 mol% Sm^{3+}-doped ceria (SDC) below 600 °C, having as a consequence the smallest ohmic resistance loss during cell discharge below 600 °C among the three electrolytes.

In the work of Iwahara et al. [46] it was found that the total conductivity of the $BaCe_{1-x}Sm_xO_{3-\delta}$ system in hydrogen atmosphere increases with the increase of samarium content and reaches a maximum approximately at $x = 0.2$. Furthermore, its values are higher than those measured for $BaCe_{0.9}Nd_{0.1}O_{3-\delta}$ and $SrCe_{0.95}Yb_{0.05}O_{3-\delta}$. Sharova et al. [45] found that the conductivity of $BaCe_{1-x}Sm_xO_{3-\delta}$ is two orders of magnitude greater than the conductivity of pure $BaCeO_3$.

In the present work samarium oxide as the dopant material was chosen and the influence of this dopant's amount on the electrical and thermal properties of the $BaCeO_3$ based electrolyte was investigated.

2. Experimental

The samarium doped barium cerates ($BaCe_{1-x}Sm_xO_{3-\delta}$) were prepared by solid-state synthesis using high-purity CeO_2, Sm_2O_3 and $BaCO_3$. The corresponding nominal formation reaction is:

$$BaCO_3 + (1-x)CeO_2 + x/2Sm_2O_3 \rightarrow BaCe_{1-x}Sm_xO_{3-\delta} + CO_2\uparrow \quad (7)$$

The powders of the initial materials were ground in the appropriate proportions and mixed in an agate mortar with ethanol for 1 h. Afterwards they were calcined at 1400 °C for 3 h with a heating and cooling rate 300 °C h^{-1}. Then the powders were ground and

prepared in the form of sheets by rolling with the addition of 5% solution of natural rubber in a mixture of acetone and gasoline (60/40). The samples of 20 mm × 5 mm × 2 mm size were cut from the sheets with subsequent calcinations for the elimination of the organic binders at 900 °C, with a heating rate of 90 °C h^{-1} and a cooling rate of 300 °C h^{-1}. Thereafter, the samples were sintered at 1600 °C for 3 h in air with a heating/cooling rate of 300 °C h^{-1}.

The phase identification of the sintered samples was investigated by employing the X-ray Diffraction technique by Cu Kα radiation (DMAX-2500, Rigaky Co. Ltd., Japan). The theoretical density of the crystals was calculated by using the formula:

$$\rho_{\text{theor}} = \frac{M}{N_a V} \tag{8}$$

where M is the molecular mass of a formula unit (g mol^{-1}), N_a the Avogadro number and V the unit cell volume (cm^3). The samples' density was calculated by the well know equation:

$$\rho = \frac{m}{V} \tag{9}$$

where m is the weight of the sample (g) and V the volume of the sample (cm^3). The relative density was calculated by the formula:

$$\rho_{\text{rel}} = \frac{\rho}{\rho_{\text{theor}}} \tag{10}$$

The microstructure of the samples, i.e. well-polished surface after thermal etching, was investigated by using the technique of Scanning Electron Microscopy (SEM) (Model: JSM-5900 LV).

The electrical conductivity measurements were carried out by employing the four-point dc technique in wet air and wet hydrogen atmosphere in the temperature range of 600–900 °C. Platinum paste stripes, deposited on the inner and outer surface of an YSZ tube and connected with platinum wires, were used as the electrochemical oxygen pump and the oxygen sensor. On the samples' surface four Pt electrodes were deposited and connected with Pt wires. The one pair was used in order to apply voltage with an electrochemical station (AMEL instruments Model 2053). The second pair of electrodes was connected to a multimeter in order to register the voltage of the samples.

The thermal expansion was measured in air during heating from 25 to 900 °C, by using a quartz dilatometer with digital micrometer on the ceramic samples $BaCe_{1-x}Sm_xO_{3-\delta}$ of 20 mm length. The micrometer sensitivity was 1 μm. The measurements were conducted both during heating and cooling process with a constant rate of 180 °C h^{-1}. The thermal expansion coefficient (TEC), α, was determined by graphic differentiation of the temperature dependence of the samples' expansion:

$$\alpha = \frac{1}{L_0}\frac{dL}{dT}\bigg|_T \tag{11}$$

where L_0 is the sample's length at room temperature.

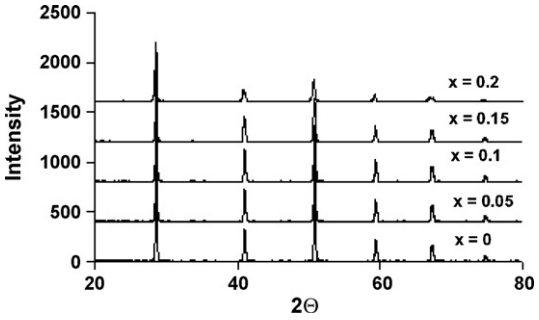

Fig. 1. XRD patterns of $BaCe_{1-x}Sm_xO_{3-\delta}$ ($0 \le x \le 0.2$) sintered at 1600 °C for 3 h.

3. Results and discussion

According to the XRD analysis (Fig. 1), at $x = 0$–0.2, the formed continuous series of solid $BaCe_{1-x}Sm_xO_{3-\delta}$ solutions have the structure of cubic perovskite with orthorhombic distortions, while the sample with $x = 0.25$ shows mixed phases of perovskite and $BaSm_2O_4$. The lattice parameters and the unit cell volume determined by the XRD analysis of the sinters are shown in Table 1. The volume of the $BaCe_{1-x}Sm_xO_{3-\delta}$ unit cell is $(340 \pm 1) \times 10^{-3}$ nm^3 and is practically independent of samarium content. The unit cell volume for $BaCe_{0.85}Sm_{0.15}O_{3-\delta}$ is equal to 340.99×10^{-3} nm^3 (Table 1), which is in accordance with the one reported in the work of Wu [52]. The synthesized ceramic was gray. Starting from $x = 0.05$, it was vacuum dense, practically without open porosity. The relative density of the samples was ~87% for $0.02 < x < 0.05$ and ~94% for $0.05 < x < 0.25$.

Based on the geometric packing of the charge spheres, the stability of the ABO_3 perovskite structure is determined from the ionic radii, r_A, r_B and r_O, and can be characterized by the Goldschmidt tolerance factor:

$$t = \frac{(r_A + r_B)}{[\sqrt{2}(r_B + r_O)]} \tag{12}$$

where r_i is the ionic radius of the i-th atom [53]. In general, the ideal cubic perovskite structure is formed when t is very close to unity. However, a large number of perovskite structures are distorted to orthorhombic, rhombohedral or tetragonal which can be approximated as cubic when t deviates from 1. In most cases, t varies between 0.75 and 1 [54]. The tolerance factors of the present $BaCe_{1-x}Sm_xO_{3-\delta}$ samples vary from $t = 0.83$ to 0.84 and are consistent with their observed non-cubic structures.

Table 1
Lattice constants and unit cell volume of the samples

x in $BaCe_{1-x}Sm_x0_{3-\delta}$	Parameters of unit cell, nm			Volume, nm
	a	b	c	
0	0.8791	0.6247	0.6206	0.34081
0.05	0.8799	0.6233	0.6218	0.34102
0.1	0.8787	0.6231	0.6214	0.34016
0.15	0.8786	0.6235	0.6224	0.34099
0.2	0.8789	0.6237	0.6226	0.34122

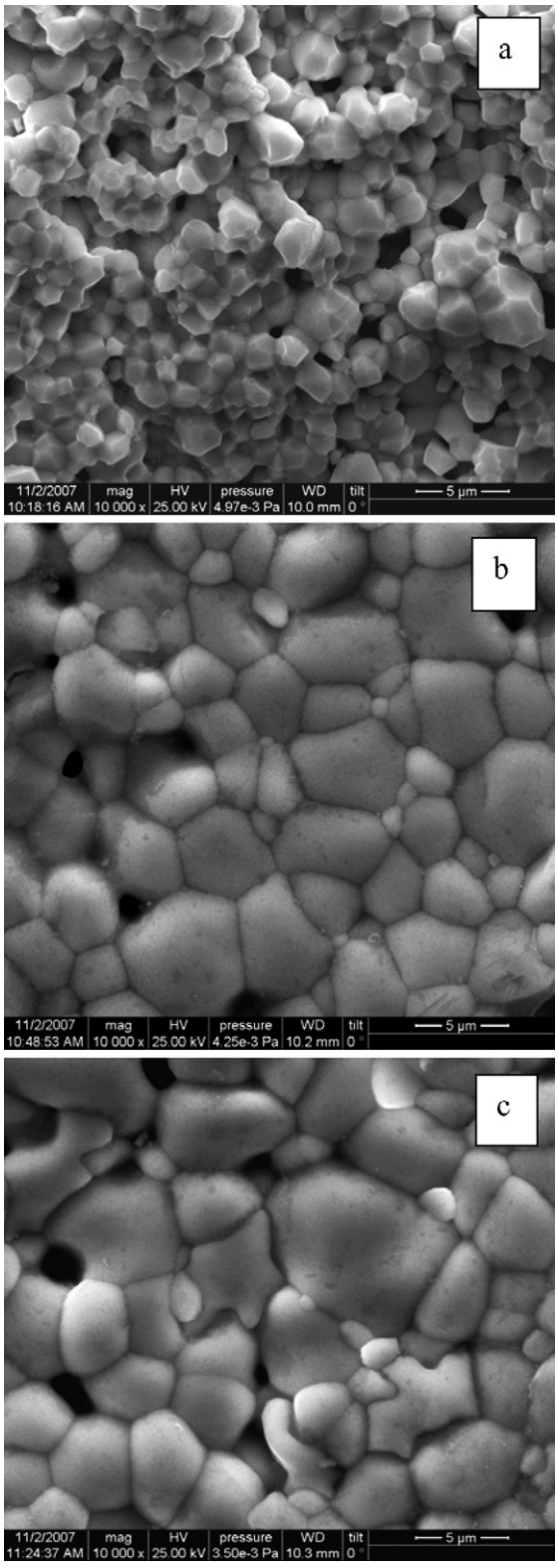

Fig. 2. SEM micrographs of the $BaCe_xSm_{1-x}O_{3-\delta}$, sintered at 1600 °C for 3 h; $BaCe_{0.95}Sm_{0.05}O_{3-\delta}$ (a), $BaCe_{0.9}Sm_{0.1}O_{3-\delta}$ (b), $BaCe_{0.85}Sm_{0.15}O_{3-\delta}$ (c).

Fig. 2 shows the SEM micrographs of $BaCe_{1-x}Sm_xO_{3-\delta}$ samples with different contents of Sm doping, i.e. 5, 10, 15 mol% (mol% refers to the cation content in B position). The $BaCe_{0.95}Sm_{0.05}O_{3-\delta}$ sample has an average grain size of

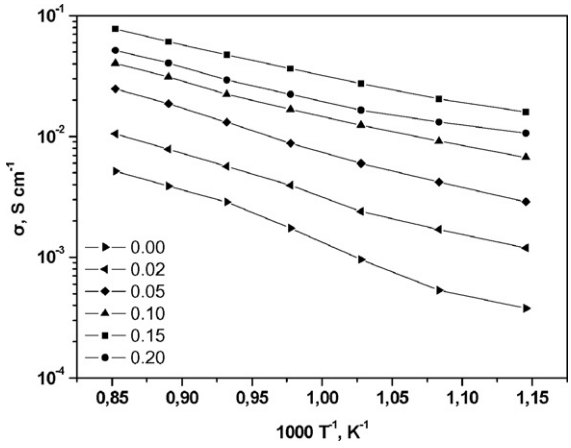

Fig. 3. Effect of temperature on the conductivity of $BaCe_{1-x}Sm_xO_{3-\delta}$ in wet air.

~1 μm, while the average grain size increases with the increase of Sm content; for $BaCe_{0.9}Sm_{0.1}O_{3-\delta}$ the average grain size is 3 μm and for $BaCe_{0.85}Sm_{0.15}O_{3-\delta}$ more than 4 μm.

As it can be seen in Fig. 3, the temperature dependences of $BaCe_{1-x}Sm_xO_{3-\delta}$ conductivity on air are in general non-linear. Their slopes decrease slightly with the decrease of temperature. The observed non-linearity may be attributed to the change of the conduction mechanism, due to the change of the ratio between the effective charge carriers' (holes, protons and oxygen ions) transfer numbers, which vary with temperature and gas composition, as well as to phase transitions. However, part of these dependencies at 600–750 °C and 750–900 °C may be considered as linear, which makes it possible to calculate the activation energy of conductivity for $BaCe_{1-x}Sm_xO_{3-\delta}$. Table 2 shows the values of activation energy calculated from the slopes of the conductivity values in wet air and in wet hydrogen atmospheres. The maximum value of conductivity in air atmosphere is reached in the case of 0.15 mol% Sm at 900 °C and corresponds to 78 mS cm^{-1}, while at the same temperature the undoped sample exhibits only 5 mS cm^{-1}.

As can someone observe in Fig. 4 the conductivity of $BaCe_xGd_{1-x}O_{3-\delta}$ in wet hydrogen increases in the same order as in air. However, the conductivity of all samples in hydrogen is lower, than the samples' conductivity in air due to the presence of hole conductivity in the latter case. In atmosphere containing oxygen with high partial pressure, these samples have revealed

Table 2
The activation energy of conduction in wet air and in wet hydrogen

x, in $BaCe_{1-x}Sm_xO_{3-\delta}$	Ea (eV) in interval of temperatures			
	600–750 °C		750–900 °C	
	Wet air	Wet H_2	Wet air	Wet H_2
0	0.790	1.220	0.741	1.460
0.02	0.600		0.677	
0.05	0.568	0.216	0.718	0.347
0.1	0.469	0.214	0.614	0.420
0.12	0.442		0.541	
0.15	0.426	0.210	0.521	0.492
0.2	0.374	0.212	0.587	0.493

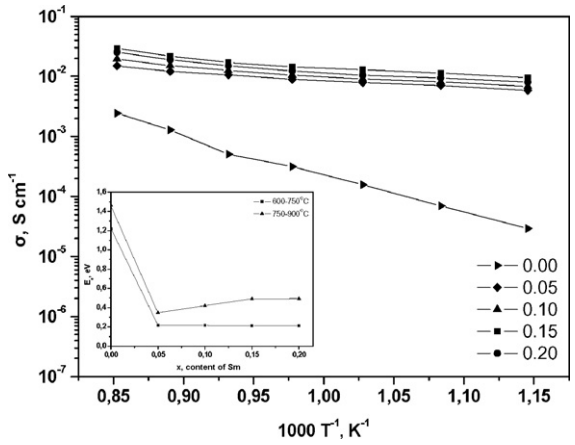

Fig. 4. Effect of temperature on the conductivity of $BaCe_{1-x}Sm_xO_{3-\delta}$ in wet hydrogen; Inset Figure: Effect of x on activation energy (E_{act}) for $BaCe_{1-x}Sm_xO_{3-\delta}$, in wet hydrogen for two temperature intervals.

a p-type conduction (hole conduction). When hydrogen is introduced into the atmosphere, the contribution of hole conduction decreases and proton conduction appears [55].

In the inset figure in Fig. 4 the activation energy is shown as a function of x for the temperature regions of 600–750 °C and 750–900 °C, because the temperature dependencies of conductivity in hydrogen may be considered as linear at these regions. In the high temperature region, E_a increases with the increase of Sm content and reaches the value of 0.49 eV at $x = 0.15$, while in the range of 600–750 °C the activation energy practically does not change. Most probably, the minor change of activation energy with the increase of Sm content in the range of 750–900 °C can be attributed to a change in the ratio between the hole, proton and oxygen transfer numbers, which can vary with the temperature change, as well as to phase transitions.

The isotherm dependence of conductivity on the dopant's concentration (x in $BaCe_{1-x}Sm_xO_{3-\delta}$) in wet hydrogen is shown in Fig. 5. At low dopant concentrations, the conductivity of the samples increases with the increase of the dopant's level and reaches its maximum values of 29 mS cm^{-1} and 9.5 mS cm^{-1} at 900 °C and 600 °C for 15 mol% Sm respectively.

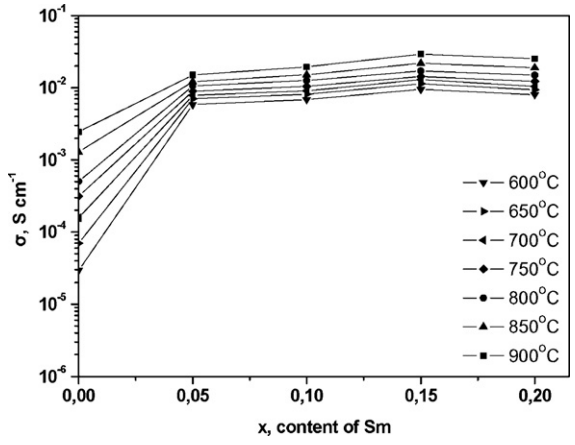

Fig. 5. Effect of Sm doping (x) on the conductivity of the $BaCe_{1-x}Sm_xO_{3-\delta}$ samples in wet hydrogen, at different temperatures.

As it was mentioned above, the total conductivity of the $BaCe_{1-x}Sm_xO_{3-\delta}$ system in wet air increases with the increase of samarium content and reaches a maximum at $x = 0.15$ with values of 0.0475 S cm^{-1} and 0.0778 S cm^{-1} at 800 °C and 900 °C, respectively (Fig. 3). The conductivity of $BaCe_{0.8}Sm_{0.2}O_{3-\delta}$ at 800 °C is considerably lower, being equal to 0.0295 S cm^{-1}. Similar data have been reported by Chakroborty et al. [44] for the same system $BaCe_{0.8}Sm_{0.2}O_{3-\delta}$; its conductivity in air was 0.0279 S cm^{-1} at 800 °C.

The observed increase of conductivity with the increase of dopant's concentration up to the composition corresponding to the maximum conductivity, can be explained by the accompanying increase in the vacancy concentration (δ in $BaCe_{1-x}Sm_xO_{3-\delta}$). An increase in free vacancy concentration generally results in enhanced ionic conductivity, although vacancy concentration has been observed to be temperature and dopant size dependent due to the dopant cation–vacancy association.

As can someone observe in Figs. 3 and 4 for compositions of x more than 0.15 the conductivity decreases noticeably as the dopant concentration increases. Wang et al. [56] supposed that the decrease in ionic conductivity after the maximum value is due to the formation of neutral complexes in the form proposed by Reichel et al. [57]: $(Y'_{Ce}V_O^{\cdot})$ or $(Y'_{Ce}V_O^{\cdot\cdot}Y'_{Ce})$. It could be assumed that these complexes are formed according to the following reactions:

$$Sm'_{Ce} + V_O^{\cdot\cdot} = (Sm'_{Ce}V_O^{\cdot\cdot})^{\cdot} \quad (13)$$

$$2Sm'_{Ce} + V_O^{\cdot\cdot} = (Sm'_{Ce}V_O^{\cdot\cdot}Sm'_{Ce}) \quad (14)$$

Similar complexes can be formed with the proton participation and they can also influence the proton (as well total) conductivity. Sharova and Golelov [58] assumed that the part of oxygen transport upon doping increases faster than that of protonic, probably because substitutional defects Nd'_{Ce} may trap protons:

$$Nd'_{Ce} + H_i^{\cdot} = [Nd'_{Ce}H_i^{\cdot}]^x \quad (15)$$

In the present case the analogical processes can take place:

$$Sm'_{Ce} + H_i^{\cdot} = [Sm'_{Ce}H_i^{\cdot}]^x \quad (16)$$

The temperature dependencies of the linear expansion of the $BaCe_{1-x}Sm_xO_{3-\delta}$ ($x = 0.5$, 0.1, 0.15, 0.2) samples in the range from room temperature up to 900 °C are shown in Fig. 6. These dependences are non-linear and the line bending increases with the dopant's content increase. One can easily distinguish a critical point around 500 °C for all samples. This critical point corresponds to the temperature of 773 K at which Knight [5] observed one of the pure $BaCeO_3$ phase transitions. Our results are also in good agreement with the results reported in the work of Yamaguchi and Yamada [59] for the Yb-doped $BaCeO_3$-system.

The dependence of thermal expansion coefficient (TEC) of the studied ceramic materials on samarium content in the temperature range of 600–900 °C are shown in Fig. 7. The TEC decreases with the samarium content increase up to $x = 0.2$. The TEC of the pure $BaCeO_3$ is $13.8 \cdot 10^{-6}$ K^{-1}, which is in accordance with the one reported in the work of Pal'guev [21]. The

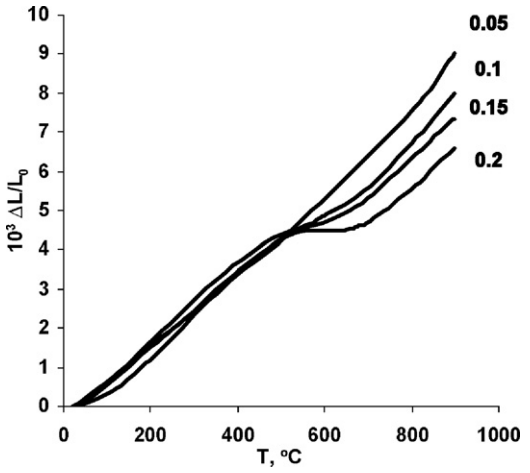

Fig. 6. Effect of temperature on the relative linear expansion of the $BaCe_{1-x}Sm_xO_{3-\delta}$ system.

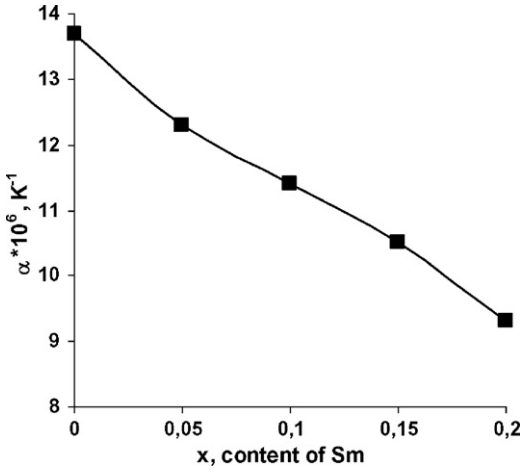

Fig. 7. Effect of samarium content on thermal expansion coefficient.

TEC of $BaCe_{0.85}Sm_{0.15}O_{3-\delta}$ is significantly smaller than that of $BaCeO_3$ and almost the same as for yttria stabilized zirconia electrolyte. However, it is not quite clear the reason why the thermal expansion coefficient of $BaCe_{1-x}Sm_xO_{3-\delta}$ decreases very rapidly with the samarium content increase.

4. Conclusions

In the present work, the novel family of $BaCe_{1-x}Sm_xO_{3-\delta}$ solid compositions with perovskite structure has been prepared as single phase compounds with samarium content up to $x = 0.2$. The temperature dependence of total conductivity in both wet air and wet hydrogen atmosphere has been studied and the activation energy values for conductivity have been determined. The effect of different samarium content on the properties of $BaCe_{1-x}Sm_xO_{3-\delta}$ have been examined. It was found that the composition $BaCe_{0.85}Sm_{0.15}O_{3-\delta}$ presents the highest conductivity in this system. The ceramic material of this composition has the same thermal expansion co-efficient as the one of the yttria stabilized zirconia electrolyte. This allows the use of the same electrode materials for a cell based on the abovementioned ceramic material as the ones for zirconia based cells, as well as the same interconnect materials.

References

[1] H. Iwahara, H. Uchida, K. Ono, K. Ogaki, J. Electrochem. Soc. 135 (1988) 529–533.
[2] H. Iwahara, H. Uchida, K. Morimoto, J. Electrochem. Soc. 137 (1990) 462–465.
[3] A. Hoffmann, Zeitschrift fuer Physikalische Chemie, Abteilung B: Chemie der Elementarprozesse, Aufbau der Materie, 28 (1935) 65–77.
[4] A.J. Jacobson, B.C. Tofield, B.E.F. Fender, Acta Crystallogr. B 28 (1972) 956–961.
[5] K.S. Knight, Solid State Ionics 74 (1994) 109–117.
[6] T. Shimura, H. Tanaka, H. Matsumoto, T. Yogo, Solid State Ionics 176 (2005) 2945–2950.
[7] T. Higuchi, T. Tsukamoto, H. Matsumoto, T. Shimura, K. Yashiro, T. Kawada, J. Mizusaki, S. Shin, T. Hattori, Solid State Ionics 176 (2005) 2967–2970.
[8] H. Zhao, M. Pijolat, J. Mater. Chem. 12 (2002) 3787–3791.
[9] E. Gorbova, D. Medvedev, A. Demin, V. Maragou, P. Tsiakaras, Proceedings of the 16th International Conference on Solid State Ionics, 1–6 July 2007, 2007, p. 598.
[10] E. Gorbova, V. Maragou, D. Medvedev, A. Demin, P. Tsiakaras, Proceedings of the Tenth Grove Fuel Cell Symposium, 25–27 September, 2007, p. 127.
[11] E. Gorbova, V. Maragou, D. Medvedev, A. Demin, P. Tsiakaras, Proceedings of the Tenth Grove Fuel Cell Symposium, 25–27 September, 2007, p. 128.
[12] E. Gorbova, V. Maragou, D. Medvedev, A. Demin, P. Tsiakaras, J. Power Sources 181 (2008) 292–296.
[13] A.N. Virkar, H.S. Maiti, J. Power Sources 14 (1985) 295–303.
[14] N. Maffei, L. Pelletier, A. McFarlan, J. Power Sources 175 (2008) 221–225.
[15] Q. Ma, R. Peng, Y. Lin, J. Gao, G. Meng, J. Power Sources 161 (2006) 95–98.
[16] L. Pelletier, A. McFarlan, N. Maffei, J. Power Sources 145 (2005) 262–265.
[17] N. Maffei, L. Pelletier, J.P. Charlan, A. McFarlan, J. Power Sources 162 (2006) 165–167.
[18] N. Maffei, L. Pelletier, J.P. Charland, A. McFarlan, J. Power Sources 140 (2005) 264–267.
[19] N. Maffei, L. Pelletier, A. McFarlan, J. Power Sources 136 (2004) 24–29.
[20] T. Shimada, C. Wen, N. Taniguchi, J. Otomo, H. Takahashi, J. Power Sources 131 (2004) 289–292.
[21] S.F. Pal'guev, Ural. Otd. Ross. Akad. Nauk, 1998.
[22] H. Iwahara, Solid State Ionics 28–30 (1988) 573–578.
[23] H. Uchida, N. Maeda, H. Iwahara, Solid State Ionics 11 (1983) 117–124.
[24] N.V. Sharova, V.P. Gorelov, Russ. J. Electrochem. 39 (2003) 461–466.
[25] R. Glockner, M.S. Islam, T. Norby, Solid State Ionics 122 (1999) 145–146.
[26] T. He, P. Ehrhart, Solid State Ionics 86-88 (1996) 633.
[27] K.D. Kreuer, Solid State Ionics 122 (1999) 285.
[28] M. Glerup, F.W. Poulsen, R.W. Berg, Solid State Ionics 148 (2002) 83.
[29] W. Munch, G. Seifert, K.D. Kreuer, J. Majer, Solid State Ionics 86-88 (1996) 621.
[30] R.C.T. Slade, N. Singh, Solid State Ionics 46 (1991) 111.
[31] T. Scherban, Yu.M. Baikov, E. Shalkova, Solid State Ionics 66 (1999) 159–164.
[32] J.R. Frade, Solid State Ionics 78 (1995) 87–97.
[33] E.O. Ahlgren, J. Phys. Chem. Solids 58 (1997) 1475–1480.
[34] H. Iwahara, Solid State Ionics 77 (1995) 289–298.
[35] A. Demin, P. Tsiakaras, Int. J. Hydrogen Energy 26 (2001) 1103–1108.
[36] A.K. Demin, P.E. Tsiakaras, V.A. Sobyanin, S.Yu. Hramova, Solid State Ionics 152–153 (2002) 555–560.
[37] A. Demin, P. Tsiakaras, E. Gorbova, S. Hramova, J. Power Sources 131 (2004) 231–236.
[38] J.B. Goodenough, Annu. Rev. Mater. Res. 33 (2003) 91–128.
[39] D. Hirabayashi, A. Tomita, S. Teranishi, T. Hibino, M. Sano, Solid State Ionics 176 (2005) 881.

[40] F.L. Chen, O.T. Sorensen, G.Y. Meng, D.K. Peng, J. Eur. Ceram. Soc. 18 (1998) 1389–1395.
[41] W. Grover Coors, W. Dennis, Readey, J. Am. Ceram. Soc. 85 (11) (2002) 2637–2640.
[42] D.A. Stevenson, N. Jiang, R.M.B. Buchanan, F.E.G. Henn, Solid State Ionics 62 (1993) 279–285.
[43] X.T. Su, Q.Z. Yan, X.H. Ma, W.F. Zhang, C.-C. Ge, Solid State Ionics 177 (2006) 1041–1045.
[44] A. Chakroborty, A. Das Sharma, B. Maiti, H.S. Maiti, Mat. Lett. 57 (2002) 862–867.
[45] N.V. Sharova, V.P. Gorelov, V.B. Balakireva, Russ. J. Electrochem. 41 (2005) 665–670.
[46] H. Iwahara, T. Yajima, T. Hibino, H. Ushida, J. Electrochem. Soc. 140 (1993) 1687–1691.
[47] P. Ranran, W. Yan, Y. Lizhai, M. Zongqiang, Solid State Ionics 177 (2006) 389–396.
[48] D. Hirabayashi, A. Tomita, S. Teranishi, T. Hibino, M. Sano, Solid State Ionics 176 (2005) 881–887.
[49] K. Jiang, Z. He, J. Meng, Y. Ren, Q. Su, Science in China, Series B Chem. 42 (1999) 298–304.
[50] B.L. Kuzin, M.V. Perfil'ev, V.P. Gorelov, S.M. Beresnev, Yu.N. Kleshchev, Russ. J. Electrochem. 33 (1997) 1371–1375.
[51] T. Hibino, A. Hashimoto, M. Suzuki, M. Sano, J. Electroch. Soc. 149 (2002) A1503–A1508.
[52] J. Wu, PhD thesis, California Institute of Technology, 2005, p. 130.
[53] Yu. Lur'e, Handbook of Analytical Chemistry, Khimiya, Moskow, 1989, p. 447.
[54] Yu.P. Vorobiov, A.N. Men', V.B. Fetisov, Calculating and Predicting Properties of Oxides, Moskow, Nauka, 1983, p. 287.
[55] G. Ma, T. Shimura, H. Iwahara, Solid State Ionics 110 (1998) 103–110.
[56] D.U. Wang, D.S. Park, J. Griffith, A.S. Nowick, Solid State Ionics 2 (1981) 95–105.
[57] U. Reichel, R.R. Arons, W. Schilling, Solid State Ionics 86–88 (1996) 639–645.
[58] N.V. Sharova, V.P. Gorelov, Russ. J. Electrochem. 41 (2005) 1001–1007.
[59] S. Yamaguchi, N. Yamada, Solid State Ionics 162–163 (2003) 23–29.